ROYAL SOCIETY
OF CHEMISTRY

PAPER

Check for updates

Proton-transfer rate constants for the determination of organic indoor air pollutants by online mass spectrometry†

Tunga Salthammer, [iD] *[a] Uwe Hohm, [iD] [b] Marcel Stahn [iD] [c] and Stefan Grimme [iD] [c]

Proton transfer reaction mass spectrometry (PTR-MS) has become an indispensable analytical tool for indoor related sciences. With high-resolution techniques not only is the online monitoring of the selected ions in the gas phase possible, but also, with some limitations, the identification of substance mixtures without chromatographic separation. The quantification is carried out with the help of kinetic laws, which require knowledge of the conditions in the reaction chamber, the reduced ion moblilities and the reaction rate constant k_{PT} under these conditions. Ion–dipole collision theory can be used to calculate k_{PT}. One approach is an extension of Langevin's equation and is known as average dipole orientation (ADO). In a further development, the analytical solution of ADO was replaced by trajectory analysis, which resulted in capture theory. The calculations according to ADO and capture theory require precise knowledge of the dipole moment and the polarizability of the respective target molecule. However, for many relevant indoor related substances, these data are insufficiently known or not known at all. Consequently, the dipole moment μ_D and polarizability α of 114 organic compounds that are frequently found in indoor air had to be determined using advanced quantum mechanical methods. This required the development of an automated workflow that performs conformer analysis before computing μ_D and α using density functional theory (DFT). Then the reaction rate constants with the H_3O^+ ion are calculated according to the ADO theory (k_{ADO}), capture theory (k_{cap}) and advanced capture theory (k_{cap}^*) for different conditions in the reaction chamber. The kinetic parameters are evaluated with regard to their plausibility and critically discussed for their applicability in PTR-MS measurements.

1 Introduction

A milestone in the analytical chemistry of the gas phase was the development of online mass spectrometry, which is, *inter alia*, suitable for numerous applications in food control, medicine and environmental research.[1,2] The method was developed for very volatile and volatile organic compounds (VVOCs and VOCs) and is preferably used when their concentration has to be determined down to the ppt range and with high time resolution. The first applications in atmospheric chemistry aimed to examine ambient air.[3–5] However, the suitability of online mass spectrometry for indoor applications was quickly recognized.[6,7] A basic distinction is made between selected ion flow tube mass spectrometry (SIFT-MS)[8] and proton-transfer-reaction mass

spectrometry (PTR-MS),[9,10] with the latter being mainly established in indoor air sciences.[7] The use of PTR-MS to analyze human respiratory gas has been known for many years.[11–13] Other successful areas of PTR-MS application and other mass spectrometry techniques with indoor-related questions involve ozone-initiated chemistry,[6,14–16] photocatalytic reactions,[17,18] measurements in museums,[19,20] exposure under living conditions[21–23] and gas phase/particle partitioning.[24]

However, online mass spectrometry has pros and cons. The coverage of a wide mass range and the high time resolution are often offset by calibration problems. In addition, only molecules whose proton affinity is greater than that of water can be studied, since H_3O^+ is the preferred reagent for proton transfer. Ions of the same nominal mass cannot be distinguished with a low-resolution quadrupole mass filter without disproportionate effort, their selective analysis requires a time-of-flight (ToF) detector. Not all molecules can be detected *via* the [M + 1]$^+$ ion but rather fragment in the reaction tube, which makes both qualification and quantification more difficult.[25,26]

In a PTR-MS system quantification takes place from the signals of the ions involved, the device settings and the reaction constant of the proton transfer k_{PT}. However, it is a fundamental problem of the PTR-MS method that reliable k_{PT} values are only

[a]Fraunhofer WKI, Department of Material Analysis and Indoor Chemistry, 38108 Braunschweig, Germany. E-mail: tunga.salthammer@wki.fraunhofer.de

[b]Institute of Physical and Theoretical Chemistry, University of Braunschweig – Institute of Technology, 38106 Braunschweig, Germany

[c]Mulliken Center for Theoretical Chemistry, Institute for Physical and Theoretical Chemistry, University of Bonn, 53115 Bonn, Germany

† Electronic supplementary information (ESI) available. See DOI: https://doi.org/10.1039/d3ra01705b

available for a comparatively small number of molecules. On the other hand, k_{PT} can theoretically be calculated. The theory of ion–polar molecule collisions developed by Su and Bowers,[27,28] also called average orientation dipole – ADO theory, is well suited for a reasonable estimation of reaction constants. In later works, Su and Chesnavich[29] have taken an alternative route. The results of trajectory calculations were parameterized to give expressions which allow the calculation of k_{PT}. This approach is known as capture theory. Finally, Su[30] parameterized the trajectory calculations for the relative kinetic energy dependence of the rate constant at various temperatures. The ADO and the capture theory were discussed and compared by Ellis and Mayhew.[31]

Whichever theory is used, precise data on the dipole moment and polarizability of the target compound under the current reaction conditions are always required. The most critical quantity is the dipole moment. Even for a small and rigid molecule like acetaldehyde, the results of quantum mechanical calculations are between 2.65 D,[32] 2.88 D[33] and 2.94 D (this work), depending on the level of theory. Generally, the span between these quantum chemically calculated dipole moments increases with molecular size and flexibility, which can be attributed to routinely considering only a single molecular geometry. This ignores conformational flexibility and thermal effects, which is far from reality. These effects can significantly impact geometries and geometry-dependent properties like dipole moments (see below). For many molecules that play a role in the indoor environment, no reliable gas phase dipole moments are known at all.

In this work, we provide quantum chemically calculated, thermally averaged ensemble dipole moments and polarizabilities for 114 organic molecules. On that basis, we calculate and discuss rate constants for proton transfer reactions of organic compounds with H_3O^+ ions according to ADO theory and capture theory. Particular attention is paid to Su's[30] advanced capture theory, because this allows the calculation of k_{PT} as

a function of the electric field strength in the PTR-MS reaction chamber. We believe that these data are of particular value for the reliable determination of organic indoor air pollutants.

2 Methods

2.1 Software

The program OriginPro 2021b (64-bit) (OriginLab, Northampton, MA) was used for all non-quantum mechanical calculations, non-linear regression analyses, statistical evaluations and the drawing of some images. ChemDraw 16.0.1.4 (PerkinElmer Informatics Inc.) was used for drawing chemical structures. DFT calculations were performed using the program package TURBOMOLE 7.5.1.[34]

2.2 Quantum chemical calculations

Density functional theory (DFT) is routinely used to calculate dipole moments and polarizabilities for organic molecules. However, these calculations need reasonable starting geometries for all investigated compounds as input. Getting these geometries by hand for 114 organic compounds is tedious work and would limit further up-scaling of the developed workflow for an even larger number of compounds. Therefore, a workflow had to be developed as a first step that allows the automatic calculation of the relevant properties from more readily available inputs, such as CAS numbers.

The PubChem[35] database provides with its Power User Gateway (PUG) an URL-based API (application programming interface) for programmatic access to its contents. Using a simple command-line program dubbed PubGrep, we were able to get reasonable starting structures for all molecules by translating the given input to a PubChem Compound Identification (CID) first and afterward getting the corresponding 3D structure information from the database. If no 3D structure information was available, the 2D structure information was taken instead and converted into a 3D structure using the 2D to
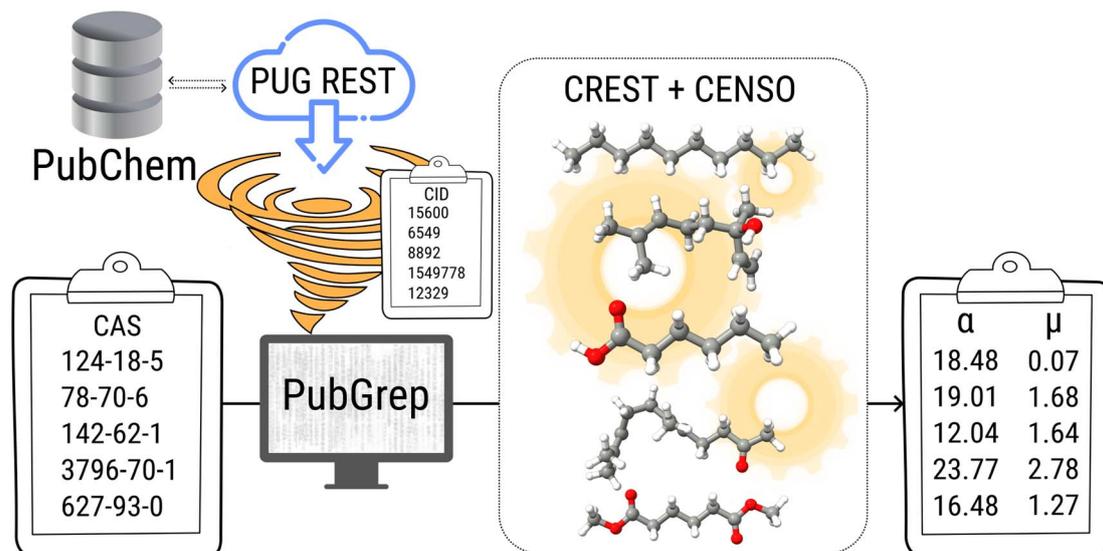

Fig. 1 Simplified schematic of the automated calculation workflow including PubGrep, CREST and CENSO.

3D structure converter included in our xTB program suite. Because dipole moments are highly dependent on the geometric structure of the molecule, a conformational sampling was performed using the program CREST[36] with the GFN2-xTB[37] semiempirical method. The resulting conformer ensemble was re-ranked with the program CENSO[38] and the r²SCAN-3c[39] composite DFT method with an energy threshold of 2.0 kcal mol^{-1} (8.4 kJ mol^{-1}). These conformer ensembles were finally used to calculate the dipole moments and polarizabilities with the ωB97X-V[40] DFT method. This functional is reported to perform very well for dipole moments with an RMS regularized error (RMSE) of just over 5% for small organic or inorganic molecules.[41] A simplified schematic of this workflow is visualized in Fig. 1. Due to the rapid convergence of the computed dipole moment with the size of the applied AO basis (remaining completeness effects of about 0.1%), the def2-TZVPP basis set was chosen for computational efficiency. Instead of just using the lowest lying conformer for these calculations, the properties were calculated as a Boltzmann-weighted average over all conformers in the DFT refined ensemble at 298.15 K up to a Boltzmann threshold of 99% as

$$\overline{\mu}_D = \sum_i^{\text{conf.}} (p_i \cdot \mu_{D_i}) \tag{1}$$

$$\overline{\alpha} = \sum_i^{\text{conf.}} (p_i \cdot \alpha_i) \tag{2}$$

with the Boltzmann-weighting factor p_i as

$$p_i = \frac{e^{\frac{-G_i}{k_B \cdot T}}}{\sum_i^{\text{conf.}} e^{\frac{-G_i}{k_B \cdot T}}}. \tag{3}$$

G_i is the DFT computed free energy of conformer i, T is the absolute temperature and k_B is the Boltzmann constant.

3 Fundamentals of PTR-MS

The principle of PTR-MS is based on chemical ionization of organic molecules. H_3O^+ ions are generated as primary reagents in an ion source. These enter the drift reaction chamber, where they collide with the sample gas molecules. In this process, a proton is transferred, resulting in the formation of ionized organic molecules and water as shown in eqn (4). Organic compounds, whose proton affinity is higher than the proton affinity of water (691 kJ mol^{-1})[42] can be measured according to this principle.

$$R + H_3O^+ \rightarrow RH^+ + H_2O \tag{4}$$

For $[H_3O^+] \gg [RH^+]$ the VOC concentration $[R]$ can be obtained from eqn (5) if the drift time t_r and the proton transfer constant k_{PT} are known.[9,10,31]

$$[R] = \frac{1}{k_{PT} \cdot t_r} \cdot \frac{[RH^+]}{[H_3O^+]} \tag{5}$$

$[RH^+]$ and $[H_3O^+]$ are the concentrations of the product and the primary ion, respectively. The drift time t_r and drift velocity v_d are related to the instrumental settings according to eqn (6).[33]

$$t_r = \frac{L_d}{v_d} = \frac{L_d^2}{U_d \cdot u_0} \cdot \frac{p_d \cdot T_0}{p_0 \cdot T_d} \tag{6}$$

L_d is the length of the drift tube, U_d the applied drift voltage, and u_0 is the reduced ion mobility,[5] which itself depends on the actual instrument settings.[3,43] T_d and p_d are the actual temperature and pressure in the drift tube, $p_0 = 101\,325$ Pa and $T_0 = 273.15$ K are the pressure and temperature at standard conditions, respectively. The conditions inside the drift tube are expressed by the ratio E/N of the electric field strength $E = U_d/L_d$ to the number density N. Assuming ideal gas behaviour we have $N = p_d/k_B T_d$ and $N_0 = p_0/k_B T_0$, k_B is the Boltzmann constant. The drift velocity v_d from eqn (6) is given by eqn (7).

$$v_d = u_0 \cdot N_0 \cdot \frac{E}{N} \tag{7}$$

Usually, the ratio E/N is expressed in Townsend (Td) where 1 Td $= 10^{-21}$ V m^2. The values of u_0 for H_3O^+ ions and the $H_3O^+ \cdot (H_2O)$ cluster were experimentally determined by Dotan et al.[43] as a function of E/N. Note that these data can also be found as a graph in Warneke et al.[3] and in the book of Ellis and Mayhew.[31] In both publications, the data from Dotan et al.[43] are discussed in detail and assessed as valid. Clusters only occur with small E/N values. For 100 Td the $H_3O^+ \cdot (H_2O)/H_3O^+$ concentration ratio is 1.1 and for 120 Td it is 0.023.[31] Table 1 shows values for u_0, v_d and t_r at different E/N with a drift tube length $L_d = 9.6$ cm. Clusters are not discussed further, the data

Table 1 Data for H_3O^+ and $H_3O^+ \cdot (H_2O)$ in the PTR-MS drift tube at $L_d = 9.6$ cm and $T_d = 353$ K. The u_0 were taken from Warneke et al.[3]

Ion	E/N T$_d$	u_0 cm^2 (V s)$^{-1}$	v_d m s^{-1}	t_r μs	KE$_{ion}$ 10^{-20} J	KE$_{ion}$ eV
H_3O^+	80	2.73	587	164	2.10	0.13
H_3O^+	90	2.74	663	145	2.47	0.15
H_3O^+	100	2.75	739	130	2.90	0.18
H_3O^+	110	2.80	828	116	3.45	0.22
H_3O^+	120	2.81	906	106	3.99	0.25
H_3O^+	130	2.85	996	96	4.67	0.29
H_3O^+	140	2.89	1087	88	5.42	0.34
$H_3O^+ \cdot H_2O$	80	2.32	499	193	1.72	0.11
$H_3O^+ \cdot H_2O$	90	2.36	571	168	2.02	0.13
$H_3O^+ \cdot H_2O$	100	2.41	648	148	2.40	0.15
$H_3O^+ \cdot H_2O$	110	2.44	721	133	2.80	0.17

are given in Table 1 for comparison. Small molecules have similar rate constants for H_3O^+ and $H_3O^+ \cdot (H_2O)$.[44] The E/N value not only affects the energy of the ions in the drift chamber, but also the fragmentation behavior of the molecules. In chemical ionization, the $[M + 1]^+$ ions are often formed preferentially, but many molecules tend to fragment, a well-studied example being terpenoids.[25,45] Normally, molecules fragment more with higher E/N. A comprehensive fragment ion database is provided by Pagonis et al.[46]

4 Determination of k_{PT} values

4.1 Calculation of the reaction rate constant k_{ADO} from dipole orientation theory

A widely used approach to calculate k_{PT} follows the ion–dipole collision theory developed by Su and Bowers.[27] Eqn (8) is an extension of Langevin's approach. The term k_L describes the classical Langevin rate coefficient for the interaction of an ion with a non-polar molecule. The contribution of the interaction between ion and dipole is given by k_{μ_D}.

$$k_{ADO} = k_L + k_{\mu_D}$$

$$k_L = \sqrt{\frac{\pi \cdot \alpha \cdot q^2}{\mu_m \cdot \varepsilon_0}} \qquad (8)$$

$$k_{\mu_D} = \frac{C \cdot q \cdot \mu_D}{\varepsilon_0} \cdot \sqrt{\frac{1}{2 \cdot \pi \cdot \mu_m \cdot k_B \cdot T}}$$

In eqn (8), q is the charge of the ion, α the polarizability of the neutral reactant with dipole moment μ_D, μ_m the reduced mass of the reactants and ε_0 the vacuum electric permittivity. C is a temperature dependent dimensionless "locking" parameter (0

$\leq C \leq 1$) that accounts for the permanent dipole moment of the molecule. All quantities are given in SI units. Conversion factors to other units as well as values of the fundamental constants are given in the ESI.†

4.2 The locking parameter C

C is a function of the dipole moment μ_D and the square root of the polarizability α of the neutral molecule. For an entirely non-polar molecule, $C = 0$ and then eqn (8) corresponds to the classical Langevin approach. Temperature-dependent values for C as a function of $\mu_D/\alpha^{1/2}$ were published by Su and Bowers[47] and Su et al.[48] The data sets for 300 K and 350 K were fitted with the empirical eqn (9) in order to be able to calculate k_{ADO} for the respective target molecules. The fit parameters are presented in Table 2, the fit curves are shown in Fig. 2 and the data are provided in the ESI (Appendix A).†

$$C = A_1 + \frac{-A_1}{1 + \left(\frac{\mu_D \cdot \alpha^{-1/2}}{A_2}\right)^p} \qquad (9)$$

Extending their ADO theory, Su et al.[48] developed an approach that takes into account the moment of inertia of a molecule. The authors explain that, strictly speaking, their extended theory only provides exact values for small linear molecules with a moment of inertia $I \leq 10^{-39}$ g cm^2. Moreover, Su et al.[48] mention that the temperature dependent C values from Su and Bowers[47] contain a "minor error". Unfortunately, corrected data for 350 K were not presented, only for 300 K (see Fig. 2B). We therefore used the data from Su and Bowers[47] in our work in order to be able to make comparisons with other k_{PT} values.

4.3 Calculation of the collision rate constant k_{cap} by trajectory analysis

An alternative to analytical expressions for calculating rate coefficients for ion–molecule interactions is to model reaction processes by trajectory calculations. Su and Chesnavich[29] have published corresponding parameterizations of this method,

Table 2 Fit parameters according to eqn (9) for the data sets $C = f(\mu_D, \alpha)$ (see ESI) at 300 K and 350 K. Here μ_D is given in Debye and α in 10^{-24} cm^3

Temperature	A_1	A_2	p	Data from ref.
300 K	0.29366	0.24274	1.10725	Su et al.[48]
350 K	0.28279	0.46805	1.56293	Su and Bowers[47]
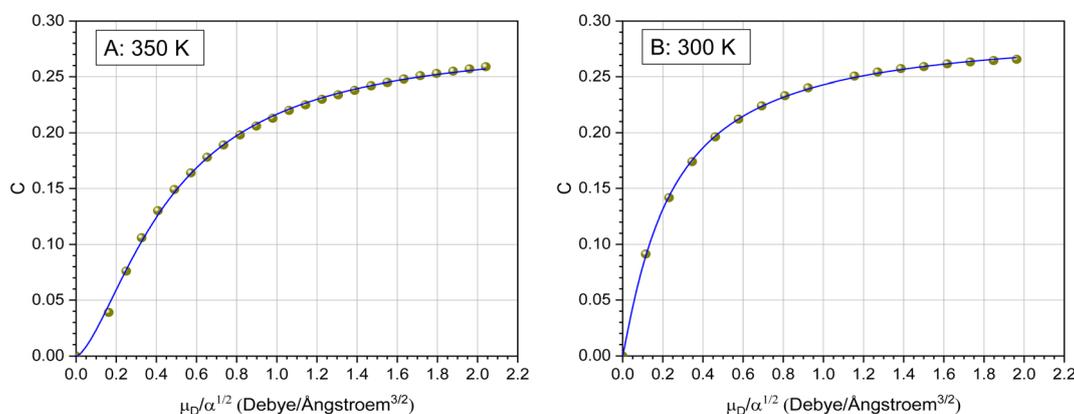
Fig. 2 Plot of the locking parameter C versus $\mu_D/\alpha^{1/2}$ and fitting curve with eqn (9). The data for 350 K (A) are from Su and Bowers[47] and the 300 K data (B) are from Su et al.[48]

known as capture theory, with which temperature-dependent rate constants can be determined. First, the reaction rate k_L according to Langevin (see eqn (8) with $C = 0$) is determined. In order to obtain the capture rate coefficient k_{cap}, k_L is multiplied by the parameterized quantity K_{cap} according to eqn (10) and (11).

$$k_{cap} = k_L \cdot K_{cap}(T_R) \tag{10}$$

$$T_R = 4 \cdot \pi \cdot \varepsilon_0 \cdot \frac{2 \cdot \alpha \cdot k_B \cdot T}{\mu_D^2} \tag{11}$$

All quantities are given in SI units. The full trajectory analysis method for K_{cap} is provided with the respective units in the ESI (Appendix B).† It is a disadvantage of Su and Chesnavich's[29] capture theory that only for small molecules K_{cap} is a function of T_R and independent of the moment of inertia I. Ellis and Mayhew[31] state that for the reactions taking place in the PTR-MS, K_{cap} is insensitive to the moment of inertia. In principle, however, this must be checked individually for each molecule. The question whether the conditions of the capture theory are fulfilled depends not only on I but also on μ_D and α. We have not performed a rigorous analysis of all the compounds being relevant here, as k_{cap} is presented and calculated for comparison purposes only.

4.4 Calculation of the collision rate constant k_{cap}^* by advanced trajectory analysis

In a later work, Su[30] presented improved parameterizations that cover a wider temperature range. This takes into account the effect that the temperature of the ions traveling along a drift tube is higher than the drift tube temperature T_d because they experience additional energy from the electric field. Eqn (12) for the total mean ion kinetic energy KE_{ion} was originally developed by Wannier[49] and later discussed by de Gouw et al.[5] in relation to PTR-MS applications.

$$KE_{ion} = \frac{3}{2} \cdot k_B \cdot T + \frac{1}{2} \cdot m_{ion} \cdot v_d^2 + \frac{1}{2} \cdot m_{air} \cdot v_d^2 \tag{12}$$

For $T = 353$ K and different E/N ratios, KE_{ion} values of H_3O^+ and $H_3O^+ \cdot H_2O$ are listed in Table 1. The collision energy of an ion–molecule reaction is then obtained from eqn (13). This is the kinetic energy KE_{CM} relative to the center of mass of the colliding system that is available for the reaction process.[31]

$$KE_{CM} = \frac{m_m}{m_m + m_{ion}} \cdot \left(KE_{ion} - \frac{3}{2} \cdot k_B \cdot T \right) + \frac{3}{2} \cdot k_B \cdot T \tag{13}$$

In eqn (12) and (13) m_{ion} is the mass of the respective ion H_3O^+ or $H_3O^+ \cdot H_2O$, m_{air} is the average mass of dry air and m_m is the mass of the target molecule. The reaction constant k_{cap}^* is then obtained according to eqn (14) from the Langevin constant k_L and the factor K_C, which according to Su[30] depends on the parameters τ and ε to be calculated from the dipole moment μ_D, polarizability α and KE_{CM}.

$$k_{cap}^* = k_L \cdot K_C(\tau, \varepsilon) \tag{14}$$

The full trajectory analysis method is provided in the ESI (Appendix C).† The influence of the kinetic energy on the reaction constant is discussed by Ellis and Mayhew[31] using acetone at 300 K as an example. The difference to thermal energy is also significant for the increased temperature in a PTR-MS drift tube (353 K was assumed here). A value of $KE_{CM} = 0.20$ eV then results for acetone at $E/N = 120$ Td, the thermal energy from $3/2 \cdot k_B \cdot T$ accounts to 0.05 eV. As already pointed out in detail by Cappellin et al.,[50] the particular advantage of k_{cap}^* is that it can be used over a wide temperature range. Moreover, there is a direct connection with the electric field in the drift tube via the drift velocity v_d, see eqn (7). This allows the rate constants to be calculated as a function of the E/N value for the respective drift tube temperature.

5 Results and discussion

5.1 Dipole moments

The essential parameters for calculating k_{ADO}, k_{cap} and k_{cap}^* are the dipole moment μ_D and the polarizability α. Both quantities are linked to the molar polarization via the Debye equation.[51] For PTR-MS measurements, values are required for the complete, thermally averaged conformer ensemble in the gas phase, because changes in the molecular geometry affect the dipole moment in particular. This effect has not been considered so far in our context. It has already been mentioned that published values can vary considerably. For gas phase 2-butoxyethanol, we calculate a dipole moment of 2.42 D after conformer analysis, while Iglesias et al.[52] published 2.13 D for this molecule in cyclohexane. For 2-ethyl-1-hexanol with a calculated gas phase dipole moment of 1.61 D and a measured dipole moment in cyclohexane of 1.69 D at 298 K[53] the difference is less pronounced. Nevertheless, it should be noted that the geometry of a molecule significantly impacts the dipole moment, and solvent interactions can influence the conformational distribution.[38] Therefore, values measured in solution are not useful for flexible molecules. For example, the absolute difference between the dipole moment for the thermally averaged conformer ensemble and the lowest-lying conformer ($\Delta \mu_D$) of 2-ethyl-1-hexanol is 0.21 D. The mean deviation of the $\Delta \mu_D$ values for all of the investigated compounds is with 0.13 D significant. The deviations are more pronounced for non-rigid molecules, such as 2-butoxyethylacetate (0.43 D), geranylacetone (0.45 D) or dimethylsebacate (1.4 D). The maximum $\Delta \mu_D$ value is as high as 2.62 D for dimethyl phthalate. Moreover, tabulated data often has the disadvantage that the experimental conditions are unknown. Reliable data are only tabulated for a limited number of molecules,[54,55] but quantum chemical tools for their calculation are nowadays routinely available.[50] In this respect, quantum mechanical calculations computed for conformer ensembles appear as the only reasonable alternative, especially in the case of large and non-rigid molecules. The polarizabilities are much less susceptible to conformer changes than the dipole moments. Since the quality of many of the

Table 3 Dipole moments, polarizabilities and calculated rate constants k_{cap}^* at 353 K in dependence of E/N for the reaction of organic compounds with H_3O^+ ions in the PTR-MS drift tube according to Su's[30] capture theory. Other parameters and rate constants are listed in the ESI

Compound	CAS	μ_D D	α 10^{-24} cm^3	k_{cap}^* 10^{-9} cm^3 s^{-1}						
				$(E/N) = 80$ Td	90	100	110	120	130	140
Aliphatic and cyclic hydrocarbons										
n-Hexane	110-54-3	0.04	11.30	1.99	1.99	1.99	1.99	1.99	1.99	1.99
n-Heptane	142-82-5	0.08	13.09	2.12	2.12	2.12	2.12	2.12	2.12	2.12
n-Octane	111-65-9	0.06	14.87	2.24	2.24	2.24	2.24	2.24	2.24	2.24
n-Nonane	111-84-2	0.08	16.66	2.35	2.35	2.35	2.35	2.35	2.35	2.35
n-Decane	124-18-5	0.07	18.48	2.46	2.46	2.46	2.46	2.46	2.46	2.46
Cyclohexane	110-82-7	0.00	10.36	1.91	1.91	1.91	1.91	1.91	1.91	1.91
Methylcyclohexane	108-87-2	0.12	12.17	2.05	2.05	2.05	2.05	2.05	2.05	2.05
4-Vinyl cyclohexene (4-VCH)	100-40-3	0.30	13.82	2.17	2.17	2.17	2.17	2.17	2.17	2.17
Aromatic hydrocarbons										
Benzene	71-43-2	0.00	10.07	1.90	1.90	1.90	1.90	1.90	1.90	1.90
Toluene	108-88-3	0.39	12.00	2.04	2.04	2.04	2.04	2.04	2.04	2.04
Ethylbenzene	100-41-4	0.42	13.80	2.17	2.17	2.17	2.17	2.17	2.17	2.17
o-Xylene	95-47-6	0.66	13.85	2.24	2.17	2.17	2.17	2.17	2.17	2.17
m-Xylene	108-38-3	0.37	13.95	2.18	2.18	2.18	2.18	2.18	2.18	2.18
p-Xylene	106-42-3	0.00	14.00	2.18	2.18	2.18	2.18	2.18	2.18	2.18
1,2,3-Trimethylbenzene	526-73-8	0.73	15.70	2.36	2.29	2.29	2.29	2.29	2.29	2.29
1,2,4-Trimethylbenzene	95-63-6	0.40	15.85	2.30	2.30	2.30	2.30	2.30	2.30	2.30
1,3,5-Trimethylbenzene	108-67-8	0.00	15.91	2.31	2.31	2.31	2.31	2.31	2.31	2.31
Isopropylbenzene	98-82-8	0.39	15.56	2.28	2.28	2.28	2.28	2.28	2.28	2.28
Styrene	100-42-5	0.17	14.43	2.22	2.22	2.22	2.22	2.22	2.22	2.22
Chlorobenzene	108-90-7	1.86	12.25	2.86	2.75	2.65	2.56	2.49	2.42	2.37
1,2-Dichlorobenzene	95-50-1	2.65	14.32	3.51	3.43	3.33	3.20	3.08	2.94	2.84
1,4-Dichlorobenzene	106-46-7	0.00	14.56	2.18	2.18	2.18	2.18	2.18	2.18	2.18
4-Phenyl cyclohexene (4-PCH)	4994-16-5	0.28	20.06	2.55	2.55	2.55	2.55	2.55	2.55	2.55
Polycyclic aromatic hydrocarbons										
Naphthalene	91-20-3	0.00	17.37	2.40	2.40	2.40	2.40	2.40	2.40	2.40
1-Methylnaphthalene	90-12-0	0.36	19.25	2.51	2.51	2.51	2.51	2.51	2.51	2.51
1-Chloronaphthalene	90-13-1	1.79	19.50	3.03	2.96	2.89	2.83	2.79	2.75	2.72
Anthracene	120-12-7	0.00	26.19	2.89	2.89	2.89	2.89	2.89	2.89	2.89
Phenanthrene	85-01-8	0.01	24.89	2.82	2.82	2.82	2.82	2.82	2.82	2.82
Terpenoids										
Isoprene	78-79-5	0.27	9.88	1.91	1.91	1.91	1.91	1.91	1.91	1.91
α-Pinene	80-56-8	0.18	16.51	2.33	2.33	2.33	2.33	2.33	2.33	2.33
β-Pinene	127-91-3	0.72	16.70	2.41	2.34	2.34	2.34	2.34	2.34	2.34
3-Carene	13466-78-9	0.17	16.74	2.35	2.35	2.35	2.35	2.35	2.35	2.35
D-Limonene	5989-27-5	0.57	17.45	2.39	2.39	2.39	2.39	2.39	2.39	2.39
α-Phellandrene	4221-98-1	0.24	17.42	2.39	2.39	2.39	2.39	2.39	2.39	2.39
Myrcene	123-35-3	0.44	18.73	2.48	2.48	2.48	2.48	2.48	2.48	2.48
β-Caryophyllene	87-44-5	0.50	25.07	2.81	2.81	2.81	2.81	2.81	2.81	2.81
Terpinolene	586-62-9	0.24	17.81	2.42	2.42	2.42	2.42	2.42	2.42	2.42
Linalool	78-70-6	1.68	19.01	2.95	2.88	2.82	2.77	2.73	2.69	2.67
α-Terpineol	98-55-5	1.52	18.02	2.79	2.74	2.69	2.65	2.62	2.59	2.57
Alcohols										
Methanol	67-56-1	1.70	3.14	2.37	2.33	2.30	2.26	2.23	2.18	2.13
Ethanol	64-17-5	1.73	4.90	2.47	2.43	2.39	2.33	2.27	2.19	2.11
1-Propanol	71-23-8	1.68	6.64	2.51	2.46	2.40	2.31	2.23	2.14	2.06
2-Propanol	67-63-0	1.69	6.66	2.52	2.47	2.41	2.32	2.24	2.15	2.07
1-Butanol	71-36-3	1.68	8.39	2.59	2.52	2.43	2.33	2.25	2.18	2.12
2-Butanol	75-65-0	1.69	8.37	2.59	2.53	2.44	2.34	2.26	2.19	2.13
2-Methyl-1-propanol	78-83-1	1.61	8.37	2.53	2.46	2.37	2.27	2.20	2.14	2.08
1-Pentanol	71-41-0	1.65	10.17	2.64	2.53	2.44	2.36	2.30	2.24	2.19
1-Hexanol	111-27-3	1.66	11.96	2.69	2.59	2.51	2.44	2.38	2.33	2.29
1-Heptanol	111-70-6	1.66	13.75	2.74	2.65	2.58	2.51	2.47	2.42	2.38
2-Ethyl-1-hexanol	104-76-7	1.61	15.37	2.75	2.68	2.62	2.56	2.52	2.48	2.45
Benzyl alcohol	100-51-6	1.62	12.68	2.67	2.58	2.51	2.44	2.40	2.35	2.31

Table 3 (Contd.)

Compound	CAS	μ_D D	α 10^{-24} cm^3	k^*_{cap} 10^{-9} cm^3 s^{-1} (E/N) = 80 Td	90	100	110	120	130	140
Aldehydes										
Acetaldehyde	75-07-0	2.94	4.45	3.40	3.33	3.26	3.19	3.13	3.07	3.02
Propanal	123-38-6	2.85	6.14	3.35	3.29	3.23	3.17	3.12	3.05	2.99
Butanal	123-72-8	2.83	7.90	3.39	3.34	3.29	3.22	3.16	3.08	2.99
2-Methylpropanal	78-84-2	2.91	7.88	3.45	3.39	3.34	3.27	3.21	3.14	3.05
Pentanal	110-62-3	2.85	9.68	3.49	3.43	3.37	3.30	3.22	3.12	3.00
Hexanal	66-25-1	2.83	11.45	3.55	3.49	3.43	3.33	3.24	3.12	2.98
Heptanal	111-71-7	2.86	13.25	3.66	3.59	3.51	3.40	3.29	3.15	3.01
Octanal	124-13-0	2.85	15.04	3.72	3.65	3.55	3.43	3.30	3.15	3.03
Nonanal	124-19-6	2.85	16.84	3.79	3.71	3.60	3.46	3.32	3.18	3.07
Decanal	112-31-2	2.85	18.66	3.86	3.76	3.64	3.49	3.35	3.22	3.12
Acrolein (trans)	107-02-8	3.43	6.34	3.84	3.76	3.68	3.60	3.54	3.47	3.41
Acrolein (cis)	107-02-8	2.81	6.14	3.33	3.27	3.22	3.16	3.11	3.04	2.97
trans-2-Butenal	123-73-9	4.20	8.40	4.48	4.38	4.29	4.19	4.11	4.03	3.95
trans-2-Hexenal	6728-26-3	4.37	12.02	4.68	4.59	4.50	4.41	4.33	4.24	4.15
Furfural (trans)	98-01-1	3.60	9.82	3.99	3.91	3.85	3.77	3.70	3.62	3.53
Furfural (cis)	98-01-1	4.31	9.88	4.51	4.41	4.32	4.22	4.15	4.07	3.98
Glyoxal (cis)	107-22-2	3.68	4.64	3.87	3.77	3.68	3.58	3.51	3.43	3.36
Benzaldehyde	100-52-7	3.42	12.53	4.01	3.95	3.88	3.79	3.71	3.60	3.47
Ketones										
Acetone	67-64-1	3.11	6.15	3.55	3.48	3.42	3.35	3.29	3.23	3.16
2-Butanone (MEK)	78-93-3	2.97	7.86	3.49	3.44	3.38	3.31	3.25	3.18	3.09
4-Methyl-2-pentanone (MIBK)	108-10-1	2.87	11.36	3.58	3.52	3.45	3.36	3.27	3.15	3.01
Cyclohexanone	108-94-1	3.45	10.57	3.93	3.86	3.79	3.72	3.65	3.56	3.45
6-Methyl-5-heptene-2-one (6-MHO)	110-93-0	2.88	15.12	3.75	3.68	3.58	3.46	3.34	3.18	3.05
4-Oxopentanal (4-OPA)	626-96-0	2.95	9.73	3.51	3.45	3.39	3.32	3.24	3.14	3.03
Geranylacetone	3796-70-1	2.78	23.77	3.98	3.85	3.69	3.54	3.44	3.34	3.25
3-Octanone	106-68-3	2.71	14.90	3.62	3.53	3.44	3.31	3.18	3.04	2.93
Esters										
Methyl acetate	79-20-9	1.88	6.77	2.61	2.56	2.50	2.42	2.34	2.23	2.14
Ethyl acetate	141-78-6	2.03	8.59	2.82	2.76	2.69	2.59	2.49	2.39	2.30
n-Butyl acetate	123-86-4	2.06	12.13	3.00	2.92	2.81	2.69	2.60	2.52	2.45
2-Ethylhexyl acetate	103-09-3	1.84	19.01	3.04	2.95	2.88	2.82	2.77	2.73	2.69
Dimethyl phthalate	131-11-3	2.93	19.46	3.91	3.81	3.68	3.52	3.39	3.26	3.15
Diethylphthalate	84-66-2	2.60	23.06	3.79	3.63	3.50	3.37	3.28	3.19	3.12
Dimethyl succinate	106-65-0	1.30	12.80	2.38	2.33	2.29	2.25	2.22	2.20	2.17
Dimethyl adipate	627-93-0	1.27	16.48	2.55	2.52	2.48	2.46	2.43	2.41	2.40
Dimethyl sebacate	106-79-6	1.50	23.76	3.01	2.97	2.93	2.90	2.88	2.86	2.84
Glycols										
2-Ethoxyethanol	110-80-5	2.45	9.20	3.16	3.10	3.04	2.95	2.87	2.76	2.63
1-Methoxy-2-propanol	107-98-2	2.33	9.16	3.07	3.01	2.95	2.86	2.77	2.65	2.53
1,2-Propanediol	57-55-6	2.34	7.29	2.97	2.93	2.87	2.80	2.74	2.64	2.54
2-Butoxyethanol	111-76-2	2.42	12.70	3.30	3.22	3.13	3.01	2.89	2.77	2.68
2-Butoxyethoxyethanol	54446-78-5	2.81	16.93	3.74	3.65	3.54	3.39	3.26	3.13	3.02
Phenoxyethanol	122-99-6	1.67	15.41	2.79	2.71	2.64	2.58	2.54	2.50	2.46
2-Butoxyethyl acetate	112-07-2	1.73	16.36	2.85	2.77	2.70	2.64	2.59	2.55	2.52
Acids										
Formic acid	64-18-6	1.56	3.30	2.13	2.10	2.07	2.02	1.98	1.92	1.86
Acetic acid	64-19-7	1.80	5.01	2.44	2.40	2.35	2.29	2.23	2.15	2.06
Propionic acid	79-09-4	1.69	6.72	2.46	2.41	2.34	2.25	2.17	2.08	2.01
Hexanoic acid	142-62-1	1.64	12.04	2.64	2.55	2.47	2.40	2.35	2.30	2.26
Isobutyric acid	79-31-2	1.74	8.45	2.59	2.52	2.44	2.33	2.25	2.18	2.11
Phenones										
Acetophenone	98-86-2	3.16	14.20	3.90	3.84	3.76	3.65	3.55	3.41	3.25
Benzophenone	119-61-9	3.11	22.62	4.19	4.08	3.95	3.77	3.63	3.49	3.38

Table 3 (*Contd.*)

Compound	CAS	μ_D D	α 10^{-24} cm^3	k_{cap}^* 10^{-9} cm^3 s^{-1} $(E/N) = 80$ Td	90	100	110	120	130	140
Darocur 1173	7473-98-5	3.89	18.41	4.55	4.47	4.38	4.27	4.16	4.01	3.84
Irgacure 184	947-19-3	3.42	22.90	4.40	4.30	4.17	4.01	3.85	3.68	3.54
Siloxanes										
D4	556-67-2	0.60	28.26	2.94	2.94	2.94	2.94	2.94	2.94	2.94
D5	541-02-6	0.86	35.16	3.26	3.26	3.26	3.26	3.26	3.26	3.26
D6	540-97-6	0.74	42.11	3.56	3.56	3.56	3.56	3.56	3.56	3.56
Other										
Acetonitrile	75-05-8	4.06	4.34	4.39	4.28	4.17	4.05	3.96	3.86	3.77
Ethylamine	75-04-7	1.37	5.55	2.27	2.21	2.15	2.07	2.00	1.93	1.87
Diethylamine	109-89-7	0.99	9.17	2.07	2.04	2.01	1.98	1.96	1.94	1.93
Triethylamine	121-44-8	0.68	12.56	2.15	2.14	2.07	2.07	2.07	2.07	2.07
Dimethyl sulfide	75-18-3	1.68	7.27	2.56	2.50	2.43	2.33	2.25	2.17	2.10
1,3-Benzothiazol	95-16-9	1.31	15.49	2.56	2.51	2.48	2.44	2.42	2.40	2.38
N-Methyl-2-pyrrolidon	872-50-4	4.12	10.28	4.38	4.29	4.21	4.12	4.05	3.97	3.88
2-Butanonoxim	96-29-7	1.04	9.54	2.09	2.05	2.02	1.99	1.97	1.95	1.94
Phenol	108-95-2	1.29	10.87	2.33	2.28	2.23	2.19	2.15	2.12	2.10

dipole moments available in the literature could not be evaluated and in order to avoid inconsistencies, only dipole moments and polarizabilities that were determined quantum mechanically according to the method described in Section 2 were used to calculate k_{ADO}, k_{cap} and k_{cap}^*. All dipole moments, polarizabilities and calculated k_{cap}^* values are listed in Table 3. The k_{ADO} and k_{cap} values are listed in the ESI† (Appendix D).

However, if one refers to the literature, the question now arises as to how precisely the dipole moment of a molecule is available for the conditions prevailing here and what range has to be expected when calculating the reaction constants. For example, experimental values of 1.84 D[55] and 1.87 D[56] in the liquid state have been published for *n*-butyl acetate. Our calculations resulted in a value of $\mu_D = 2.06$ D. The difference between experiment (liquid phase) and theory (gas phase) is striking but not surprising. Dipole moments in gas phase and liquid phase are hardly comparable. Molecular geometries are impacted by dispersion and solvent interactions and will therefore often look very different in these phases, changing the resulting dipole moments.

Attig *et al.*[57] calculated dipole moments of *n*-butyl acetate using quantum mechanical methods with 18 different levels of theory. The minima and maxima were 1.97 D and 2.35 D, respectively. However, these values are obtained only for the lowest-lying conformer and are not directly comparable to our thermally averaged results over a conformer ensemble. The computed dipole moment for the lowest-lying conformer in our ensemble is 2.15 D, *i.e.*, very close to the calculated value of Attig *et al.*[57] (2.18 D) using the B3LYP/6-311++G(d,p) level of theory, which is arguably the best of their methods. A more recent benchmark study on the accuracy of dipole moments for DFT calculations[41] suggests a root mean square error (RMSE) of about 5% for the here employed method (see Section 2.1) which is quite close to the assumption by Cappellin *et al.*[50] regarding

the uncertainty in the quantum chemical calculation for the dipole moment.

Fig. 3 shows the dependence of the k_{PT} values, which were calculated with the three methods presented, on the dipole moment using the example of *n*-butyl acetate. For comparison with our value of 2.06 D, the experimentally determined dipole moments in cyclohexane[55,56] and calculated dipole moments by Attig *et al.*[57] for three assigned conformers were taken. Regardless of the calculation method, the rate constants for this
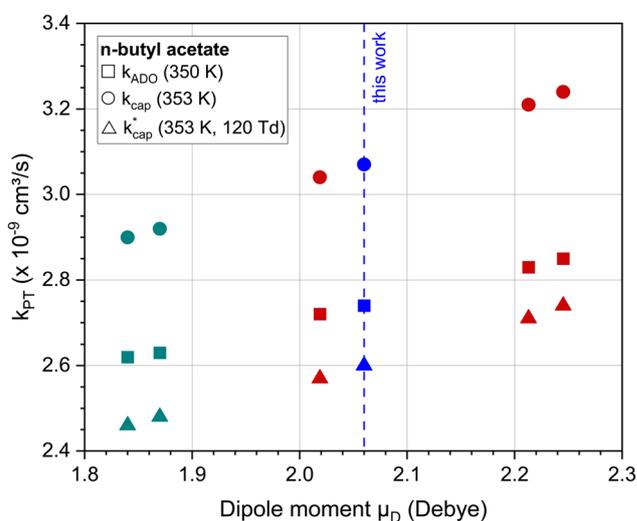

Fig. 3 Rate constants k_{ADO}, k_{cap} and k_{cap}^* for the reaction of *n*-butyl acetate with H_3O^+ ions as a function of the dipole moment. For all calculations the polarizability was $\alpha = 12.13 \cdot 10^{-24}$ cm^3. The values of 1.84 D[55] and 1.87 D[56] (green) are in cyclohexane (note: these data are used for purposes of comparison only); 2.06 D (blue) is this work; 2.02 D, 2.21 D and 2.25 D (red) are calculated data from Attig *et al.*[57] for three assigned conformers.
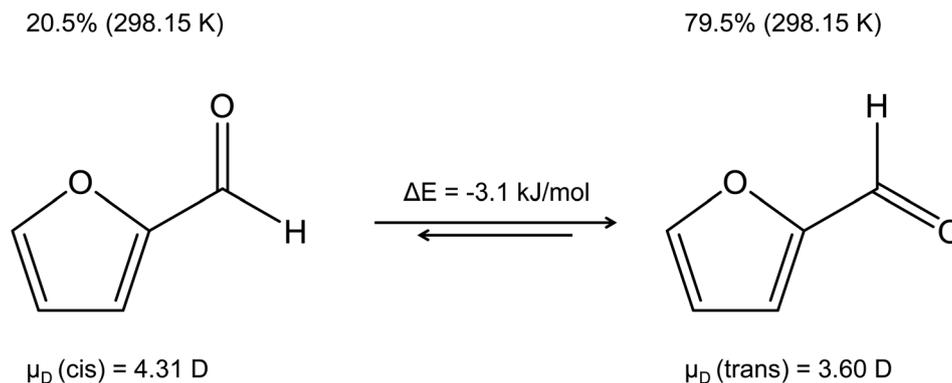
20.5% (298.15 K)　　　　　　　　　79.5% (298.15 K)

$\Delta E = -3.1$ kJ/mol

μ_D (cis) = 4.31 D　　　　　　　　μ_D (trans) = 3.60 D

Fig. 4　Dipole moments of the cis and trans isomers of furfural in the gas phase,[58] percent of each isomer, and the energy difference between the two conformers.[59]

molecule vary by 5–10% when the dipole moments differ by about 10%. However, it should be noted that uncertainties in the polarizability were not considered. For *n*-butyl acetate, Fig. 3 shows reasonable values for the dependence of k_{PT} on the dipole moment. However, the results must not be generalized, since higher dipole moments have a greater influence on k_{PT}. The differences between the calculation methods are discussed in Section 5.2.

The reliability of theoretical k_{PT} calculations stands and falls not only with the precision of the dipole moment and the polarizability, but it is also important to get the "right" molecule. The question may therefore arise as to which isomer a dipole moment is to be calculated for. A good example is furfural shown in Fig. 4, whose dominant trans isomer at 298.15 K has a calculated dipole moment of 3.60 D, while 4.31 D is given for the cis isomer.[58] Moreover, the energy of the trans isomer is 3.1 kJ mol^{-1} lower than that of the cis isomer.[59] A similar case concerns acrolein with the more abundant cis isomer[60] (μ_D(cis) = 2.81 D). The dipole moment of the trans isomer is μ_D(trans) = 3.43 D. Acrolein was already discussed in a previous publication.[61]

5.2　Reaction rate constants

Application of the ion–dipole collision theory is the most common method for determining k_{PT} in PTR-MS and SIFT measurements. It should only be mentioned at this point that other formulas can be used to calculate reaction constants in related techniques such as multiple-ion laminar flow tube spectrometry (MIFT).[62,63]

Zhao and Zhang[32] provide k_{ADO} values at 300 K for a total of 136 substances. However, Cappellin *et al.*[33] doubt that these data can be used for PTR-MS applications and argue with the electric field strength, which induces far more energetic collisions than those at room temperature. Blake *et al.*[10] point out that the ADO theory tends to result in lower rate constants than experimentally determined k_{PT} values. With reference to Wannier[49] it is assumed that the effective temperature for ion–molecule collisions is higher than the temperature in the drift tube. For an ion with a drift velocity in the range of 900 m s^{-1}, the thermal energy accounts for only a small part of the total

kinetic energy. The calculation of the k_{ADO} data listed in the ESI† was carried out according to Su and Bowers[27,28] using their data for the locking parameter C at 350 K,[47] a common temperature for PTR-MS measurements. It was already mentioned that Su *et al.* critically discussed these data in a later publication.[48]

Ellis and Mayhew[31] also state that the ADO theory underestimates experimental k_{PT} values at 300 K, but found good agreement with k_{cap} values calculated according to Su and Chesnavich.[29] This is not surprising, because only molecules with small moments of inertia I were included in the comparisons. The molecule with the highest molecular weight was toluene. Nevertheless, Ellis and Mayhew[31] come to the reasonable conclusion that the theoretical values are just as reliable as the experimental values and that uncertainties of 20–30% must generally be expected. The k_{cap} values for the 114 target compounds of this work are listed in the ESI† (Appendix D) and were calculated for 353 K according to Su and Chesnavich.[29] The parameterizations for determining $K_{cap}(T_R)$ are also listed in the ESI.†

The ion–dipole collision theories used here have already been discussed by several authors,[9,10,31,50] but essentially for small molecules. Tsikritea *et al.*[64] state that the ADO theory and the capture theory according to Su and Chesnavich[29] are appropriate when the rotational constants of the molecules are high. Calculated k_{PT} of larger molecules relevant for the indoor environment has only rarely been compared with experimental data, but the available results are satisfactory. Strictly speaking, on account of their symmetry, none of the molecules relevant to indoor analysis as well as those listed in Table 3 meet the preconditions of Su and Chesnavich.[29] However, assuming the molecules to be linear rotors, the parameterization provided by Su[30] is reasonable and the calculation of k_{cap}^* should yield reliable results. The calculated values show the expected E/N dependent deviation from k_{cap} (see Fig. 5).

In general, one must be very careful and critical when comparing calculated and experimentally determined k_{PT} values. The rate constants depend not only on the temperature T_d in the reaction chamber, but also on the pressure p_d and in particular on the electric field in the drift tube, because these
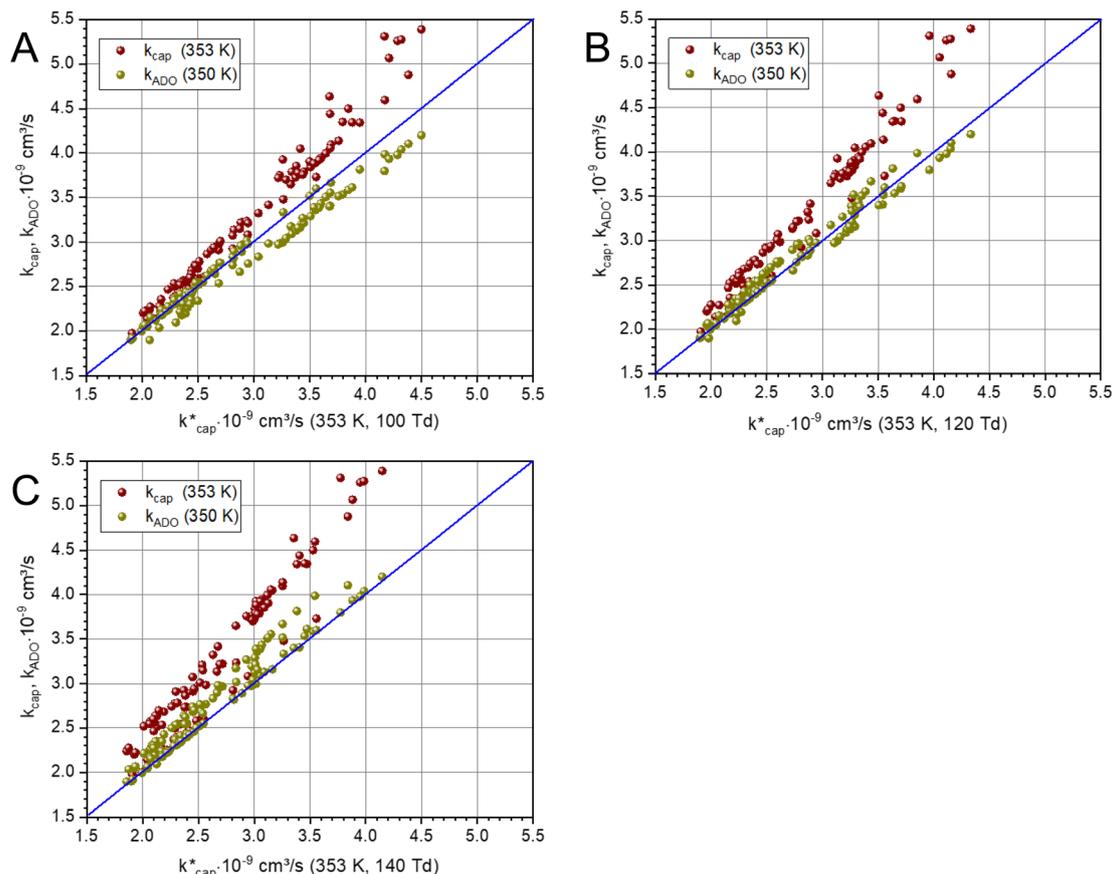
Fig. 5 Plot of k_{ADO} and k_{cap} *versus* k_{cap}^* at a temperature of 353 K (350 K for k_{ADO}) for E/N values of 100 Td (A), 120 Td (B), and 140 Td (C). The data were taken from Table 3 and from the ESI.†

variables have a direct influence on the ion mobility. The advanced capture theory takes these aspects into account. The ion energies KE_{ion} required to calculate the k_{cap}^* values listed in Table 3 are based on the ion mobilities measured by Dotan *et al.*[43] (see Table 1). The details of the parameterization for calculating k_{cap}^* from $K_C(\tau, \varepsilon)$ can be found in the ESI.† In total, k_{cap}^* was calculated for seven different E/N values between 80 Td and 140 Td at a temperature of 353 K. The advantages of Su's[30] advanced capture theory over ADO theory and the original capture theory were discussed in detail by Cappellin *et al.*[50] Using the example of seven sulfur compounds, it was also shown that the k_{cap}^* values are larger than the k_{ADO} values. In a later work, Cappellin *et al.*[33] measured k_{PT} values at $E/N = 120$ Td and $T_d = 363$ K for 11 substances that also play a role indoors. Excellent agreement with the calculated k_{cap}^* values for these conditions was found. In all cases, the deviations between theory and experiment were less than 10%. Cappellin *et al.*[33] also provide an extensive table of calculated k_{cap}^* values of organic compounds at 363 K as a function of E/N. Table 3 in this work essentially extends the list of Cappellin *et al.*[33] with a large number of indoor-related compounds. In addition, as already mentioned, the applied quantum mechanical method for calculating dipole moments and polarizabilities is superior to previous approaches.

As far as our results are concerned, there is the expected good agreement with the data of Cappellin *et al.*[33] The small deviations ($\leq 5\%$) are due to the different data for dipole moment and polarizability as well as the different temperature (353 K *vs.* 363 K). The deviations in furfural are due to the fact that Cappellin *et al.*[33] confused the dipole moments for the cis and trans isomer. The rate constants for glyoxal in Cappellin *et al.*[33] are for the trans isomer and in our work for the cis isomer.

Of particular interest is the comparison of the different theories. For this purpose, k_{ADO} and k_{cap} are plotted *versus* k_{cap}^* in Fig. 5, for 100 Td, 120 Td and 140 Td, respectively. The blue line represents the 1 : 1 ratio. It can be seen that at 100 Td the k_{ADO} values are slightly below the k_{cap}^* values from about 3.0×10^{-9} cm³ s⁻¹. At 120 Td the agreement between k_{cap}^* and k_{ADO} is excellent, at 140 Td the k_{ADO} values deviate slightly upwards. Referring to the values shown in Fig. 5, the highest differences between k_{cap}^* and k_{ADO} for 100 Td and 140 Td are in the range of 10%, for 120 Td they are $\leq 5\%$. In this respect, for our assumed conditions and substances, we cannot confirm the statement by Ellis and Mayhew[31] that ADO theory generally tends to underestimate the rate coefficients.

A different picture emerges for k_{cap}. In the three cases displayed, the calculated k_{cap} values are well above the 1 : 1 line and show the expected systematic deviations from k_{cap}^*. However, in

the case of $u_0 = $ constant, both k_{cap} and k_{cap}^* do well agree within $\approx \pm 10\%$ in the limit $E/N \to 0$. Hence, the advanced trajectory analysis and its parametrization with a field dependent kinetic energy term has proven to be a sound and reasonable extension of the capture theory. In contrast to k_{ADO}, the deviations of k_{cap} to k_{cap}^* increase with increasing rate constant and E/N. The highest deviations of about 30% occur at 140 Td with strongly polar substances such as acetonitrile, N-methyl-2-pyrrolidone and cis-furfural. In general, it is clear that deviations become more likely with increasing polarity and moment of inertia of the substance. For $\mu_D \to 0$ all theories merge into the Langevin equation. In addition, the capture theory according to Su and Chesnavich[29] has methodological weaknesses when applied to larger molecules. In the calculation of the trajectories Chesnavich *et al.*[65] have approximated all molecules as linear rotors irrespective of their effective symmetry. This means at least that the individual moments of inertia of the three mutually perpendicular axes of the molecule are averaged, which is a rough approximation for large molecules.

6 Conclusion

Proton transfer rate constants, which are necessary for the quantitative determination of airborne organic compounds in PTR-MS measurements, were calculated for 114 indoor air pollutants using ion–dipole collision theory at different levels. It was shown that this requires reliable dipole moments and polarizabilities, which are accessible for the respective ensemble containing the energetically lowest conformers in the gas phase *via* quantum mechanical calculations. The automation of these methods is necessary in order to be able to process a large number of molecules in a reasonable amount of time. In agreement with earlier work we conclude that the advanced capture theory according to Su[30] provides the most reliable rate constants k_{cap}^*, since the conditions in the PTR-MS reaction chamber are taken into account with the energy of the ions KE_{ion}, as is the E/N ratio. However, the ion mobilities in the reaction chamber as a function of E/N are required for the calculation.[3,43] For $T_d = 353$ K and $E/N = 120$ Td, the ADO theory also provides reasonable values.

After analyzing the available experimental and theoretical data, we also agree with previous estimates that the rate constants can be determined with an accuracy of 10–25%. The uncertainties increase with the size of the molecule and increasing dipole moment. For more precise assessments, round-robin tests with certified gas standards are also required, which are not yet available for PTR-MS measurements.

Author contributions

TS: conceptualization, methodology, investigation, formal analysis, visualization, writing – original draft; UH: methodology, investigation, formal analysis, verification, writing – original draft; MS: methodology, investigation, formal analysis, visualization, software, writing – original draft; SG: investigation, methodology, writing – review & editing.

Conflicts of interest

The authors have no conflicts of interest to declare.

References

1 W. Lindinger, A. Hansel and A. Jordan, On-line monitoring of volatile organic compounds at pptv levels by means of proton-transfer-reaction mass spectrometry (PTR-MS) medical applications, food control and environmental research, *Int. J. Mass Spectrom. Ion Processes*, 1998, **173**, 191–241.

2 A. Hansel, A. Jordan, R. Holzinger, P. Prazeller, W. Vogel and W. Lindinger, Proton transfer reaction mass spectrometry: on-line trace gas analysis at the ppb level, *Int. J. Mass Spectrom. Ion Processes*, 1995, **149–150**, 609–619.

3 C. Warneke, C. van der Veen, S. Luxembourg, J. de Gouw and A. Kok, Measurements of benzene and toluene in ambient air using proton-transfer-reaction mass spectrometry: calibration, humidity dependence, and field intercomparison, *Int. J. Mass Spectrom.*, 2001, **207**, 167–182.

4 A. Tani, S. Hayward and C. Hewitt, Measurement of monoterpenes and related compounds by proton transfer reaction-mass spectrometry (PTR-MS), *Int. J. Mass Spectrom.*, 2003, **223–224**, 561–578.

5 J. de Gouw, C. Warneke, T. Karl, G. Eerdekens, C. van der Veen and R. Fall, Sensitivity and specificity of atmospheric trace gas detection by proton-transfer-reaction mass spectrometry, *Int. J. Mass Spectrom.*, 2003, **223–224**, 365–382.

6 A. Wisthaler, G. Tamás, D. P. Wyon, P. Strøm-Tejsen, D. Space, J. Beauchamp, A. Hansel, T. D. Märk and C. J. Weschler, Products of ozone-initiated chemistry in a simulated aircraft environment, *Environ. Sci. Technol.*, 2005, **39**, 4823–4832.

7 T. Schripp, S. Etienne, C. Fauck, F. Fuhrmann, L. Märk and T. Salthammer, Application of proton-transfer-reaction-mass-spectrometry for indoor air quality research, *Indoor Air*, 2014, **24**, 178–189.

8 D. Smith and P. Španěl, Selected ion flow tube mass spectrometry (SIFT-MS) for on-line trace gas analysis, *Mass Spectrom. Rev.*, 2005, **24**, 661–700.

9 J. de Gouw and C. Warneke, Measurements of volatile organic compounds in the earth's atmosphere using proton-transfer-reaction mass spectrometry, *Mass Spectrom. Rev.*, 2007, **26**, 223–257.

10 R. S. Blake, P. S. Monks and A. M. Ellis, Proton-transfer reaction mass spectrometry, *Chem. Rev.*, 2009, **109**, 861–896.

11 J. Herbig, M. Müller, S. Schallhart, T. Titzmann, M. Graus and A. Hansel, On-line breath analysis with PTR-TOF, *J. Breath Res.*, 2009, **3**, 027004.

12 K. Schwarz, W. Filipiak and A. Amann, Determining concentration patterns of volatile compounds in exhaled breath by PTR-MS, *J. Breath Res.*, 2009, **3**, 027002.

13 U. Riess, U. Tegtbur, C. Fauck, F. Fuhrmann, D. Markewitz and T. Salthammer, Experimental setup and analytical methods for the non-invasive determination of volatile organic compounds, formaldehyde and NO in exhaled human breath, *Anal. Chim. Acta*, 2010, **669**, 53–62.

14 C. J. Weschler, A. Wisthaler, S. Cowlin, G. Tamás, P. Strøm-Tejsen, A. T. Hodgson, H. Destaillats, J. Herrington, J. J. Zhang and W. W. Nazaroff, Ozone-initiated chemistry in an occupied simulated aircraft cabin, *Environ. Sci. Technol.*, 2007, **41**, 6177–6184.

15 A. Wisthaler and C. J. Weschler, Reactions of ozone with human skin lipids: Sources of carbonyls, dicarbonyls, and hydroxycarbonyls in indoor air, *Proc. Natl. Acad. Sci. U. S. A.*, 2010, **107**, 6568–6575.

16 Y. Liu, P. K. Misztal, C. Arata, C. J. Weschler, W. W. Nazaroff and A. H. Goldstein, Observing ozone chemistry in an occupied residence, *Proc. Natl. Acad. Sci. U. S. A.*, 2021, **118**, e2018140118.

17 J. Mo, Y. Zhang, Q. Xu, Y. Zhu, J. J. Lamson and R. Zhao, Determination and risk assessment of by-products resulting from photocatalytic oxidation of toluene, *Appl. Catal., B*, 2009, **89**, 570–576.

18 B. Kolarik, P. Wargocki, A. Skorek-Osikowska and A. Wisthaler, The effect of a photocatalytic air purifier on indoor air quality quantified using different measuring methods, *Build. Environ.*, 2010, **45**, 1434–1440.

19 D. Pagonis, D. J. Price, L. B. Algrim, D. A. Day, A. V. Handschy, H. Stark, S. L. Miller, J. de Gouw, J. L. Jimenez and P. J. Ziemann, Time-resolved measurements of indoor chemical emissions, deposition, and reactions in a university art museum, *Environ. Sci. Technol.*, 2019, **53**, 4794–4802.

20 D. J. Price, D. A. Day, D. Pagonis, H. Stark, A. V. Handschy, L. B. Algrim, S. L. Miller, J. A. de Gouw, P. J. Ziemann and J. L. Jimenez, Sources of Gas-Phase Species in an Art Museum from Comprehensive Real-Time Measurements, *ACS Earth Space Chem.*, 2021, **5**, 2252–2267.

21 K. Kristensen, D. M. Lunderberg, Y. Liu, P. K. Misztal, Y. Tian, C. Arata, W. W. Nazaroff and A. H. Goldstein, Sources and dynamics of semivolatile organic compounds in a single-family residence in northern California, *Indoor Air*, 2019, **29**, 645–655.

22 Y. Liu, P. K. Misztal, J. Xiong, Y. Tian, C. Arata, R. J. Weber, W. W. Nazaroff and A. H. Goldstein, Characterizing sources and emissions of volatile organic compounds in a northern California residence using space- and time-resolved measurements, *Indoor Air*, 2019, **29**, 630–644.

23 D. M. Lunderberg, P. K. Misztal, Y. Liu, C. Arata, Y. Tian, K. Kristensen, R. J. Weber, W. W. Nazaroff and A. H. Goldstein, High-resolution exposure assessment for volatile organic compounds in two California residences, *Environ. Sci. Technol.*, 2021, **55**, 6740–6751.

24 L. B. Algrim, D. Pagonis, J. A. Gouw, J. L. Jimenez and P. J. Ziemann, Measurements and modeling of absorptive partitioning of volatile organic compounds to painted surfaces, *Indoor Air*, 2020, **30**, 745–756.

25 S. D. Maleknia, T. L. Bell and M. A. Adams, PTR-MS analysis of reference and plant-emitted volatile organic compounds, *Int. J. Mass Spectrom.*, 2007, **262**, 203–210.

26 P. Misztal, M. Heal, E. Nemitz and J. Cape, Development of PTR-MS selectivity for structural isomers: Monoterpenes as a case study, *Int. J. Mass Spectrom.*, 2012, **310**, 10–19.

27 T. Su and M. T. Bowers, Theory of ion–polar molecule collisions. Comparison with experimental charge transfer reactions of rare gas ions to geometric isomers of difluorobenzene and dichloroethylene, *J. Chem. Phys.*, 1973, **58**, 3027–3037.

28 T. Su and M. T. Bowers, Ion–Polar molecule collisions: the effect of ion size on ion–polar molecule rate constants; the parameterization of the average-dipole-orientation theory, *Int. J. Mass Spectrom. Ion Phys.*, 1973, **12**, 347–356.

29 T. Su and W. J. Chesnavich, Parametrization of the ion–polar molecule collision rate constant by trajectory calculations, *J. Chem. Phys.*, 1982, **76**, 5183–5185.

30 T. Su, Parametrization of kinetic energy dependences of ion–polar molecule collision rate constants by trajectory calculations, *J. Chem. Phys.*, 1994, **100**, 4703.

31 A. M. Ellis and C. A. Mayhew, *Proton Transfer Reaction Mass Spectrometry: Principles and Applications*, John Wiley & Sons, Chichester, 2013.

32 J. Zhao and R. Zhang, Proton transfer reaction rate constants between hydronium ion (H_3O^+) and volatile organic compounds, *Atmos. Environ.*, 2004, **38**, 2177–2185.

33 L. Cappellin, T. Karl, M. Probst, O. Ismailova, P. M. Winkler, C. Soukoulis, E. Aprea, T. D. Märk, F. Gasperi and F. Biasioli, On quantitative determination of volatile organic compound concentrations using proton transfer reaction time-of-flight mass spectrometry, *Environ. Sci. Technol.*, 2012, **46**, 2283–2290.

34 R. Ahlrichs, M. Bär, M. Häser, H. Horn and C. Kölmel, Electronic structure calculations on workstation computers: The program system turbomole, *Chem. Phys. Lett.*, 1989, **162**, 165–169.

35 S. Kim, J. Chen, T. Cheng, A. Gindulyte, J. He, S. He, Q. Li, B. A. Shoemaker, P. A. Thiessen, B. Yu, L. Zaslavsky, J. Zhang and E. E. Bolton, PubChem in 2021: new data content and improved web interfaces, *Nucleic Acids Res.*, 2021, **49**, D1388–D1395.

36 P. Pracht, F. Bohle and S. Grimme, Automated exploration of the low-energy chemical space with fast quantum chemical methods, *Phys. Chem. Chem. Phys.*, 2020, **22**, 7169–7192.

37 C. Bannwarth, S. Ehlert and S. Grimme, GFN2-xTB – An Accurate and Broadly Parametrized Self-Consistent Tight-Binding Quantum Chemical Method with Multipole Electrostatics and Density-Dependent Dispersion Contributions, *J. Chem. Theory Comput.*, 2019, **15**, 1652–1671.

38 S. Grimme, F. Bohle, A. Hansen, P. Pracht, S. Spicher and M. Stahn, Efficient quantum chemical calculation of structure ensembles and free energies for nonrigid molecules, *J. Phys. Chem. A*, 2021, **125**, 4039–4054.

39 S. Grimme, A. Hansen, S. Ehlert and J.-M. Mewes, r2SCAN-3c: A "Swiss army knife" composite electronic-structure method, *J. Chem. Phys.*, 2021, **154**, 064103.

40 N. Mardirossian and M. Head-Gordon, ωb97X-V: A 10-parameter, range-separated hybrid, generalized gradient approximation density functional with nonlocal correlation, designed by a survival-of-the-fittest strategy, *Phys. Chem. Chem. Phys.*, 2014, **16**, 9904–9924.

41 D. Hait and M. Head-Gordon, How accurate is density functional theory at predicting dipole moments? An assessment using a new database of 200 benchmark values, *J. Chem. Theory Comput.*, 2018, **14**, 1969–1981.

42 E. P. L. Hunter and S. G. Lias, Evaluated gas phase basicities and proton affinities of molecules: an update, *J. Phys. Chem. Ref. Data*, 1998, **27**, 413–656.

43 I. Dotan, D. L. Albritton, W. Lindinger and M. Pahl, Mobilities of CO_2^+, N_2H^+, H_3O^+, $H_3O^+ H^2O$ and $H_3O^+(H_2O)_2$ ions in N_2, *J. Chem. Phys.*, 1976, **65**, 5028–5030.

44 D. K. Bohme, G. I. Mackay and S. D. Tanner, An experimental study of the gas-phase kinetics of reactions with hydrated H_3O^+ ions ($n = 1$–3) at 298 K, *J. Am. Chem. Soc.*, 1979, **101**, 3724–3730.

45 A. Tani, Fragmentation and reaction rate constants of terpenoids determined by proton transfer reaction–mass spectrometry, *Environ. Control Biol.*, 2013, **51**, 23–29.

46 D. Pagonis, K. Sekimoto and J. de Gouw, A library of proton-transfer reactions of H_3O^+ ions used for trace gas detection, *J. Am. Soc. Mass Spectrom.*, 2019, **30**, 1330–1335.

47 T. Su and M. T. Bowers, Parameterization of the average dipole orientation theory: temperature dependence, *Int. J. Mass Spectrom. Ion Phys.*, 1975, **17**, 211–212.

48 T. Su, E. C. F. Su and M. T. Bowers, Ion–polar molecule collisions. Conservation of angular momentum in the average dipole orientation theory. The AADO theory, *J. Chem. Phys.*, 1978, **69**, 2243–2250.

49 G. H. Wannier, On the motion of gaseous ions in a strong electric field, *Phys. Rev.*, 1951, **83**, 281–289.

50 L. Cappellin, M. Probst, J. Limtrakul, F. Biasioli, E. Schuhfried, C. Soukoulis, T. D. Märk and F. Gasperi, Proton transfer reaction rate coefficients between H3O+ and some sulphur compounds, *Int. J. Mass Spectrom.*, 2010, **295**, 43–48.

51 P. W. Atkins, J. Paula and J. Keeler, *Physical Chemistry*, Oxford University Press, Oxford, 2018.

52 T. P. Iglesias, Â. F. S. Santos, F. J. V. Santos, M. L. C. J. Moita, I. M. S. Lampreia and J. C. R. Reis, Dipole moments of isomeric alkoxyalcohols in cyclohexane. Comparison of

53 Hedestrand and Fröhlich procedures with a new formula, *Phys. Chem. Chem. Phys.*, 2012, **14**, 16400.

53 A. Ghanadzadeh, H. Ghanadzadeh, R. Sariri and L. Ebrahimi, Dielectric study of molecular association in the binary mixtures (2-ethyl-1-hexanol+alcohol) and (cyclohexane+alcohol) at 298.2 K, *J. Chem. Thermodyn.*, 2005, **37**, 357–362.

54 R. D. Nelson, D. R. Lide and A. A. Maryott, *Selected values of electric dipole moments for molecules in the gas phase*, National Bureau of Standards: Washington D.C., 1967.

55 C. L. Yaws and P. K. Narasimhan, Dipole moment—Organic compounds, in *Thermophysical Properties of Chemicals and Hydrocarbons*, ed. C. L. Yaws, William Andrew Publishing, Norwich, NY, 2009, pp. 672–682.

56 J. R. Rumble, T. J. Bruno and M. J. Doa, *Handbook of Chemistry and Physics*, CRC Press, Boca Raton, 101st edn, 2020.

57 T. Attig, L. Sutikdja, R. Kannengießer, I. Kleiner and W. Stahl, The microwave spectrum of n-butyl acetate, *J. Mol. Spectrosc.*, 2013, **284–285**, 8–15.

58 K. K. Baldridge, V. Jonas and A. D. Bain, Ground state gas and solution phase conformational dynamics of polar processes: Furfural systems, *J. Chem. Phys.*, 2000, **113**, 7519–7529.

59 H. Ashish and P. Ramasami, Rotational barrier and thermodynamical parameters of furfural, thiofurfural, and selenofurfural in the gas and solution phases: theoretical study based on density functional theory method, *Mol. Phys.*, 2008, **106**, 175–185.

60 C. E. Blom, G. Grassi and A. Bauder, Molecular structure of s-cis- and s-trans-acrolein determined by microwave spectroscopy, *J. Am. Chem. Soc.*, 1984, **106**, 7427–7431.

61 A. Schieweck, E. Uhde and T. Salthammer, Determination of acrolein in ambient air and in the atmosphere of environmental test chambers, *Environ. Sci.: Processes Impacts*, 2021, **23**, 1729–1746.

62 B. Huang, H. Wu, M. Yang and Z. Luo, An integrated instrument of a tandem quadrupole mass spectrometer for cluster reaction and soft-landing deposition, *Rev. Sci. Instrum.*, 2022, **93**, 113307.

63 B. Huang, W. Gan, K. Hansen and Z. Luo, What determines the drastic reactivity of Nb_n^+ clusters with nitric oxide under thermalized conditions?, *J. Phys. Chem. A*, 2022, **126**, 4801–4809.

64 A. Tsikritea, J. A. Diprose, T. P. Softley and B. R. Heazlewood, Capture theory models: An overview of their development, experimental verification, and applications to ion–molecule reactions, *J. Chem. Phys.*, 2022, **157**, 060901.

65 W. J. Chesnavich, T. Su and M. T. Bowers, Collisions in a noncentral field: A variational and trajectory investigation of ion–dipole capture, *J. Chem. Phys.*, 1980, **72**, 2641–2655.